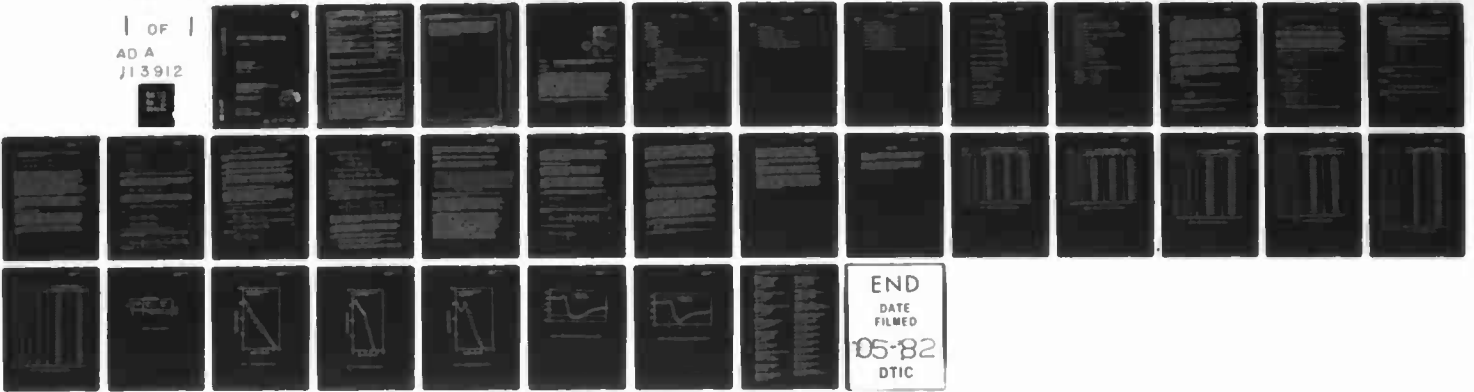


AD-A113 912 PENNSYLVANIA STATE UNIV UNIVERSITY PARK APPLIED RESE--ETC F/G 20/4  
COMPARISON OF PARABOLIZED VORTICITY AND NAVIER-STOKES SOLUTIONS--ETC(U)  
UNCLASSIFIED FEB 82 G H HOFFMAN N00024-79-C-6043  
ARL/PSU/TM-82-72 NL

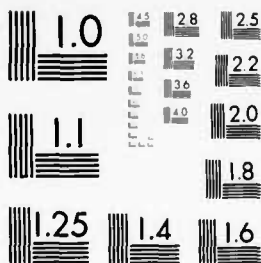
| OF |  
AD A  
J13912



1 OF 1

AD A

113912



MICROCOPY RESOLUTION TEST CHART  
NATIONAL BUREAU OF STANDARDS-1963-A

AL A 113912

6

COMPARISON OF PARABOLIZED VORTICITY AND NAVIER-STOKES SOLUTIONS IN A MILDLY NONORTHOGONAL COORDINATE SYSTEM

G. H. Hoffman

Technical Memorandum  
File No. TM 82-72  
17 February 1982  
Contract No. N000-79-C-6043

Copy No. 10

The Pennsylvania State University  
Intercollege Research Programs and Facilities  
APPLIED RESEARCH LABORATORY  
Post Office Box 30  
State College, PA 16801

Approved for Public Release  
Distribution Unlimited

DTIC  
SELECTED  
APR 28 1982  
S D  
H

NAVY DEPARTMENT  
NAVAL SEA SYSTEMS COMMAND

DTIC FILE COPY

82 04 27 160

UNCLASSIFIED

SECURITY CLASSIFICATION OF THIS PAGE (When Date Entered)

ARH/PSM/ REPORT DOCUMENTATION PAGE		READ INSTRUCTIONS BEFORE COMPLETING FORM
1. REPORT NUMBER TM 82-72	2. GOVT ACCESSION NO. AD A113 912	3. RECIPIENT'S CATALOG NUMBER
4. TITLE (and Subtitle) COMPARISON OF PARABOLIZED VORTICITY AND NAVIER-STOKES SOLUTIONS IN A MILDLY NONORTHOGONAL COORDINATE SYSTEM		5. TYPE OF REPORT & PERIOD COVERED Technical Memorandum
		6. PERFORMING ORG. REPORT NUMBER
7. AUTHOR(s) G. H. Hoffman		8. CONTRACT OR GRANT NUMBER(s) N00024-79-C-6043
9. PERFORMING ORGANIZATION NAME AND ADDRESS Applied Research Laboratory P. O. Box 30 State College, PA 16801		10. PROGRAM ELEMENT, PROJECT, TASK AREA & WORK UNIT NUMBERS
11. CONTROLLING OFFICE NAME AND ADDRESS Naval Sea Systems Command - Code NSEA-63R31 Department of the Navy Washington, DC 20362		12. REPORT DATE 17 February 1982
		13. NUMBER OF PAGES 30
14. MONITORING AGENCY NAME & ADDRESS (if different from Controlling Office)		15. SECURITY CLASS. (of this report) UNCLASSIFIED
		15a. DECLASSIFICATION/DOWNGRADING SCHEDULE
16. DISTRIBUTION STATEMENT (of this Report) Approved for Public Release. Distribution Unlimited. Per NAVSEA- April 12, 1982.		
17. DISTRIBUTION STATEMENT (of the abstract entered in Block 20, if different from Report)		
18. SUPPLEMENTARY NOTES		
19. KEY WORDS (Continue on reverse side if necessary and identify by block number)  two-dimensional, laminar flow, navier-stokes, parabolized, vorticity, solutions		
20. ABSTRACT (Continue on reverse side if necessary and identify by block number)  Two-dimensional, steady, incompressible, laminar flow in a diffuser and nozzle is considered as a model problem. A sheared mapping is used to provide a rectangular, wall-fitted, computational domain. This transformation produces a mildly nonorthogonal coordinate system in which the Navier-Stokes equations and parabolized vorticity approximation are solved. The discretization uses fourth-order accurate polynomial splines to resolve the wall boundary layer with a relatively sparse grid and standard finite differences (Continued)		

DD FORM 1473  
1 JAN 73

EDITION OF 1 NOV 65 IS OBSOLETE

UNCLASSIFIED

SECURITY CLASSIFICATION OF THIS PAGE (When Date Entered)

UNCLASSIFIED

SECURITY CLASSIFICATION OF THIS PAGE(When Data Entered)

20 - Continued

in the main stream direction. The spline-finite difference equations are solved by line relaxation and Newton-Raphson iteration. Comparison of Navier-Stokes and parabolized vorticity results are presented for two diffusers (both with separation and reattachment of the boundary layer) and one nozzle flow. The parabolized and Navier-Stokes solutions are found to be in excellent agreement. Comparisons with a published parabolized result are also given.

UNCLASSIFIED

SECURITY CLASSIFICATION OF THIS PAGE(When Data Entered)

Accession For	
NTIS GRA&I	<input checked="" type="checkbox"/>
DTIC TAB	<input type="checkbox"/>
Unannounced	<input type="checkbox"/>
Justification	
By _____	
Distribution/	
Availability Codes	
Avail and/or	
Dist	Special
A	



Subject: Comparison of Parabolized Vorticity and Navier-Stokes Solutions in a Mildly Nonorthogonal Coordinate System

References: See Page 18.

Abstract:

Two-dimensional, steady, incompressible, laminar flow in a diffuser and nozzle is considered as a model problem. A sheared mapping is used to provide a rectangular, wall-fitted, computational domain. This transformation produces a mildly nonorthogonal coordinate system in which the Navier-Stokes equations and parabolized vorticity approximation are solved. The discretization uses fourth-order accurate polynomial splines to resolve the wall boundary layer with a relatively sparse grid and standard finite differences in the main stream direction. The spline-finite difference equations are solved by line relaxation and Newton-Raphson iteration. Comparison of Navier-Stokes and parabolized vorticity results are presented for two diffusers (both with separation and reattachment of the boundary layer) and one nozzle flow. The parabolized and Navier-Stokes solutions are found to be in excellent agreement. Comparisons with a published parabolized result are also given.

Acknowledgment: This work was sponsored by the Naval Sea Systems Command, Code NSEA-63R31.

TABLE OF CONTENTS

	<u>Page</u>
ABSTRACT . . . . .	1
ACKNOWLEDGMENT . . . . .	1
LIST OF FIGURES . . . . .	3
LIST OF TABLES . . . . .	4
NOMENCLATURE . . . . .	5
I. INTRODUCTION . . . . .	7
II. ANALYSIS . . . . .	7
Governing Equations . . . . .	7
Numerical Treatment . . . . .	9
Equations at a Map Junction . . . . .	10
Vorticity Equations One Step Downstream of a Map Junction . . . . .	12
III. NUMERICAL RESULTS . . . . .	13
Problem Geometry and Numerical Solution Procedure . . . . .	13
Comparison of Navier-Stokes and Parabolized Vorticity Approximation Solutions . . . . .	14
Comparison with Results of Inoue . . . . .	15
IV. CONCLUSIONS . . . . .	16
REFERENCES . . . . .	18
FIGURES . . . . .	25

LIST OF FIGURES

<u>Figure</u>		<u>Page</u>
1.	Problem Geometry . . . . .	25
2.	Convergence History, Case 1 . . . . .	26
3.	Convergence History, Case 2 . . . . .	27
4.	Convergence History, Case 3 . . . . .	28
5.	Wall Friction Coefficient Comparison, Case 4 . . . . .	29
6.	Wall Friction Coefficient Comparison, Case 5 . . . . .	30



LIST OF TABLES

<u>Table</u>		<u>Page</u>
1.	Problem Parameters . . . . .	14
2.	Wall Friction Coefficient, Case 1 . . . . .	19
3.	Wall Pressure Coefficient, Case 1 . . . . .	20
4.	Wall Friction Coefficient, Case 2 . . . . .	21
5.	Wall Pressure Coefficient, Case 2 . . . . .	22
6.	Wall Friction Coefficient, Case 3 . . . . .	23
7.	Wall Pressure Coefficient, Case 3 . . . . .	24
8.	Diffuser Parameters for Comparison with Inoue . . . . .	16

## NOMENCLATURE

$$c_f \quad \text{wall friction coefficient} = \frac{\tau_w^*}{\frac{1}{2} \rho^* U_\infty^{*2}}$$

$$c_{p_w} \quad \text{wall pressure coefficient} = \frac{p_w^*}{\frac{1}{2} \rho^* U_\infty^{*2}}$$

$$l^\psi \quad \text{spline derivative approximation of } \frac{\partial \psi}{\partial n}$$

$$l^\zeta \quad \text{spline derivative approximation of } \frac{\partial \zeta}{\partial n}$$

$$L^\psi \quad \text{spline derivative approximation of } \frac{\partial^2 \psi}{\partial n^2}$$

$$L^\zeta \quad \text{spline derivative approximation of } \frac{\partial^2 \zeta}{\partial n^2}$$

$L^*$  reference length (dimensional)

$n$  transformed normal coordinate

$\Delta n$  step size in  $n$ -direction

$p_w^*$  wall static pressure (dimensional)

$$\text{Re} \quad \text{Reynolds number} = \frac{U_\infty^* L^*}{\nu^*}$$

RF1 relaxation factor for  $\psi$  and  $l^\psi$

RF2 relaxation factor for  $\zeta$  and  $l^\zeta$

$s$  transformed axial coordinate

$\Delta s$  step size in  $s$ -direction

$U_{\infty}^*$  free-stream speed (dimensional)  
 $x$  axial coordinate  
 $x_0$  axial coordinate of start of computational domain  
 $x_f$  axial coordinate of end of computational domain  
 $y$  normal coordinate  
 $y_e$  normal coordinate of outer edge of computational domain  
 $y_w$  normal coordinate of wall  
 $\psi$  stream function  
 $\zeta$  vorticity magnitude  
 $\tau_w^*$  wall shear stress (dimensional)  
 $\nu^*$  kinematic viscosity (dimensional)  
 $\rho^*$  fluid density (dimensional)

All other quantities are defined in the text.

All quantities in the text are made dimensionless as follows:

distances	by	$L^*$
velocities	by	$U_{\infty}^*$
stream function	by	$L^* U_{\infty}^*$
vorticity	by	$U_{\infty}^*/L^*$

I. INTRODUCTION

In Reference 1 a model strong interaction problem for two-dimensional, incompressible, laminar flow was solved numerically. The treatment involved a coupled solution of the stream function equation and a parabolized form of the vorticity equation. Fourth-order accurate polinomial splines were used to resolve the wall boundary layer with a relatively sparse grid while finite differences were used in the other direction. The geometry considered was a diffuser or nozzle made up of two flat plates connected by a cubic midsection. To produce a rectangular computational domain, a simple sheared mapping was used. Then on this mapped domain, the coupled spline-finite difference equations were solved by line relaxation plus Newton-Raphson iteration to take care of the nonlinearity.

In this report the full Navier-Stokes equations are solved for the problem of Reference 1 using the same numerical approach. The aim is to assess the effect of the mild nonorthogonality of the shearing transformation on the parabolized vorticity approximation. As part of this assessment, a slightly different parabolization is used from that of Reference 1 (the details are given in Section II).

When this work was nearly completed, a similar study came to light performed by Inoue in Japan [2].\* Inoue treats laminar, incompressible, two-dimensional flow in a diffuser using the displacement body approach coupled with a sheared mapping and standard finite difference discretization in both coordinate directions. He also uses a parabolized vorticity approximation, but different from the one used here.

The numerical results presented in this report provide an assessment of the effect of a non-optional coordinate system with mild nonorthogonality on the parabolized vorticity approximation. In addition, comparisons with the results of Inoue [2] are given.

II. ANALYSIS

Governing Equations

Under the following shearing transformation

$$s = x \quad , \quad (1)$$

$$n = \frac{y - y_w(x)}{y_e - y_w(x)} \quad , \quad (2)$$

the two-dimensional, steady, incompressible Navier-Stokes equations in stream function-vorticity form become:

---

\*Numbers in brackets [ ] indicate References. See Page 18.

$$\psi_{ss} + 2n_x \psi_{sn} + (n_y^2 + n_x^2) \psi_{nn} + n_{xx} \psi_n + \zeta = 0 \quad , \quad (3)$$

Vorticity

$$n_y (\psi_n \zeta_s - \zeta_n \psi_s) = \frac{1}{\text{Re}} [\zeta_{ss} + \underline{2n_x \zeta_{sn}} + (n_x^2 + n_y^2) \zeta_{nn} + n_{xx} \zeta_n] \quad , \quad (4)$$

where subscripts denote differentiation with respect to the subscripted variable. Neglect of the underlined diffusion terms in Eq. (4) gives the parabolized form of the vorticity equation, the same as used in Reference 1.

The transformation, Eqs. (1) and (2), is identical to that used by Inoue [2]. A slightly different transformation was used in Reference 1 where  $s$  was taken to be the wall arc length. The purpose of the shearing transformation is to map the diffuser geometry, sketched in Figure 1, into a rectangle on which a finite-difference grid can be easily superposed.

The boundary conditions to be used are also the same as in Reference 1, namely:

On the initial line,  $s = s_0$  ,  $0 \leq n \leq 1$  .

$$\left. \begin{aligned} \psi &= \psi(s_0, n) = \psi_0 \\ \zeta &= \zeta(s_0, n) = \zeta_0 \end{aligned} \right\} \quad , \quad (5)$$

where  $(\psi, \zeta)_0$  are obtained from the Blasius solution.

On the wall,  $n = 0$  ,  $s_0 \leq s \leq s_f$ .

$$\psi(s, 0) = \psi_n(s, 0) = 0 \quad , \quad (6)$$

On the diffuser centerline,  $n = 1$  ,  $s_0 \leq s \leq s_f$ ,

$$\left. \begin{aligned} \psi(s, 1) &= \psi_e(s) \\ \zeta(s, 1) &= 0 \end{aligned} \right\} \quad , \quad (7)$$

On the downstream boundary,  $s = s_f$  ,  $0 \leq n \leq 1$ ,

$$\left. \begin{aligned} \psi_{ss}(s_f, n) &= 0 \\ \zeta_{ss}(s_f, n) &= 0 \end{aligned} \right\} \quad , \quad (8)$$

In the parabolic approximation, the condition on  $\zeta$  at  $s_f$  is not needed.

Numerical Treatment

The discretization of the Navier-Stokes equations employed in this study is as follows:

1. Second-order accurate finite differences are used in the s-direction with a constant step size  $\Delta s$ . Central difference formulas are used for all s derivatives except for the convective terms in the vorticity equation where a three-point backward difference formula is used to maintain stability.
2. Fourth-order accurate spline approximations are used in the n direction with a variable step size  $\Delta n$ .

If the following spline derivatives are defined:

$$\left. \begin{aligned} \ell\psi &= \psi_n \quad , \\ L\psi &= \psi_{nn} \quad , \\ \ell\zeta &= \zeta_n \quad , \\ L\zeta &= \zeta_{nn} \quad , \end{aligned} \right\} \quad , \quad (9)$$

and the cross derivative is treated as  $\ell_s$ , then Eqs. (3) and (4) become:

Stream Function

$$\psi_{ss} + 2n_x \ell_s \psi + (n_x^2 + n_y^2) L\psi + n_{xx} \ell^2 \psi + \zeta = 0 \quad , \quad (10)$$

Vorticity

$$n_y (\ell^2 \zeta_s - \ell \zeta_s) = \frac{1}{Re} [\zeta_{ss} + 2n_x \ell_s \zeta + (n_x^2 + n_y^2) L\zeta + n_{xx} \ell^2 \zeta] \quad . \quad (11)$$

All boundary conditions remain as before except the no-slip condition which now reads

$$\ell\psi(s,0) = 0 \quad . \quad (12)$$

A rectangular grid is next placed over the computational domain with nodal points located according to,

$$\left. \begin{aligned} s_i &= (i - 1) \Delta s & , & & s_0 \leq s_i \leq s_f \\ n_{j+1} &= n_j + \Delta n_j & , & & 0 \leq n_j \leq 1 \end{aligned} \right\} \quad (13)$$

Then Eqs. (10) and (11) are discretized at  $(i,j)$  as previously described. As in Reference 1, the unknowns at  $(i,j)$  are  $\psi$ ,  $\ell\psi$ ,  $L^\psi$ ,  $\zeta$ ,  $\ell\zeta$  and  $L^\zeta$ . The two discretized equations of motion must therefore be supplemented by four spline relations. In this case,  $S^1(4,0)$ , spline 4, is used four times. The number of unknowns at  $(i,j)$  is then reduced from six to four by use of the discretized form of Eqs. (10) and (11) to eliminate  $L^\psi$  and  $L^\zeta$ . At each interior node point a coupled system of nonlinear algebraic equations results. The system of equations is completed by writing the boundary conditions in spline variables. At the wall, one two-point spline relation is required to close the system while at the diffuser centerline, two two-point spline relations must be used. These relations are given in Reference 1. At the downstream boundary, because of Eq. (8), the coefficients in the spline-finite difference (SFD) equations considerably simplify.

This algebraic system is solved by straightforward line relaxation with sweeps in the direction of  $s$  increasing using Newton-Raphson iteration at each  $s = \text{constant}$  line to take care of the nonlinearity. Thus, the numerical treatment and solution procedure of the full Navier-Stokes equations is identical to the method used for the parabolized vorticity approximation in Reference 1.

#### Equations at a Map Junction

At a junction in the mapping, which occurs at the leading or trailing edge of the diffuser, the metric coefficient  $n_{xx}$  is discontinuous because  $y_w''$  is discontinuous. Thus, a special form of the SFD stream function and vorticity equations is required. The procedure for obtaining this special form is the same as in Reference 1, but is presented here in a different manner to clarify the nature of the SFD equation at such a discontinuity.

At a map junction,  $\zeta$  and its  $x$  and  $y$  derivatives of all orders are continuous. If  $i = IJ$  is the location of the junction and superscripts  $(\ell)$  and  $(r)$  denote left and right limits at  $IJ$ , then the continuity conditions lead to

$$\zeta_{IJ}^{(\ell)} = \zeta_{IJ}^{(r)} = \zeta_{IJ} \quad , \quad (14a)$$

$$\ell \zeta_{IJ}^{(\ell)} = \ell \zeta_{IJ}^{(r)} = \ell \zeta \quad , \quad (14b)$$

$$L \zeta_{IJ}^{(\ell)} = L \zeta_{IJ}^{(r)} = L \zeta \quad , \quad (14c)$$

$$(\zeta_s)_{IJ}^{(\ell)} = (\zeta_s)_{IJ}^{(r)} \quad . \quad (14d)$$

The simple form of these relations occurs because we have a weak discontinuity; namely, in  $y_w$  only.

To make use of continuity of  $\zeta_s$ , we extend each region one step  $\Delta s$  into the other and introduce two lines of fictitious (or analytically extended) nodes, denoted by an asterisk superscript. Thus, Eq. (14d) can be approximated by central differences and after simplification yields:

$$\zeta_{IJ-1,j}^{*(r)} + \zeta_{IJ+1,j}^{*(\ell)} = \zeta_{IJ-1,j} + \zeta_{IJ+1,j} \quad . \quad (15)$$

The special form of the vorticity equation on IJ is obtained as follows: Noting that at IJ,  $n_x = 0$  and  $n_y$  is continuous, we write the vorticity equation in regions  $(\ell)$  and  $(r)$  at IJ and form the average, making use of the continuity relations (14a)-(14c). The result is:

$$[n_y (\ell \psi_{\zeta_s} - \ell \zeta_s \psi_s)]_{IJ,j} = \frac{1}{\text{Re}} [\bar{\zeta}_{ss} + n_y^2 L \zeta + \bar{n}_{xx} \ell \zeta]_{IJ,j} \quad , \quad (16)$$

where

$$(\bar{\zeta}_{ss})_{IJ,j} = \frac{1}{2} [\zeta_{ss}^{(\ell)} + \zeta_{ss}^{(r)}]_{IJ,j} \quad , \quad (17)$$

$$(\bar{n}_{xx})_{IJ,j} = \frac{1}{2} [n_{xx}^{(\ell)} + n_{xx}^{(r)}]_{IJ,j} \quad . \quad (18)$$

Thus, the map discontinuity is reflected in  $\bar{n}_{xx}$  at (IJ,j).

Next,  $\bar{\zeta}_{ss}$  is approximated by central differences using the fictitious node lines with the result,

$$[\bar{\zeta}_{ss}]_{IJ,j} = \frac{1}{2\Delta s^2} [\zeta_{IJ-1,j} + \zeta_{IJ+1,j} - 4\zeta_{IJ,j} + \zeta_{IJ-1,j}^{*(r)} + \zeta_{IJ+1,j}^{*(\ell)}] \quad ,$$

and making use of Eq. (15), the above simplifies to



$$[\bar{\zeta}_{ss}]_{IJ,j} = \frac{\zeta_{IJ-1,j} - 2\zeta_{IJ,J} + \zeta_{IJ+1,j}}{\Delta s^2} \quad (19)$$

In the present case,  $(\bar{\zeta}_{ss})_{IJ,j}$  reduces to the standard central difference formula which uses points from both regions as though no discontinuity existed.

The convective terms in Eq. (16) involve only first derivatives of  $\psi$  and  $\zeta$  with respect to  $s$ . For these derivatives three-point backward difference formulas are used which make use of nodal values in region ( $\ell$ ) only.

Derivation of the special form of the stream function equation at IJ is practically identical to the above except convective terms are absent.

The parabolization of the vorticity equation at IJ can be achieved in two ways. The first method, used in Reference 1, is to use only the equation in region ( $\ell$ ) and drop  $\zeta_{ss}^{(\ell)}$ . The second method, which takes into account the influence of both regions, is to use the averaged form Eq. (16), and omit  $\bar{\zeta}_{ss}$ .

Vorticity Equation One Step Downstream of a Map Junction

In the SFD form of the vorticity equation one step downstream of a map junction ( $i = IJ + 1$ ) second-order accuracy in the convective terms can be maintained by using the proper values of  $\psi$  and  $\zeta$  at  $(i-2,j)$  required by the three-point backward difference formulas. Since we are in region ( $r$ ), these values lie on the fictitious nodal line in ( $r$ ) one step upstream of the map junction. To obtain these values, we proceed as follows:

First, define a two-component column vector  $z$  by

$$z^T = [\psi, \zeta] \quad (20)$$

Then continuity of  $z_x$  at IJ, when put into finite difference form, leads to

$$z_{IJ-1,j}^{*(r)} + z_{IJ+1,j}^{*(\ell)} = z_{IJ-1,j} + z_{IJ+1,j} \quad (21)$$

Continuity of  $z_{xx}$ , noting that  $(n_x)_{IJ} = 0$ , leads to the additional relation,

$$(z_{ss} + n_{xx} \ell^z)_{IJ,j}^{(\ell)} = (z_{ss} + n_{xx} \ell^z)_{IJ,j}^{(r)} \quad (22)$$

Making use of

$$(\ell^z)_{IJ,j}^{(\ell)} = (\ell^z)_{IJ,j}^{(r)} = \ell^z_{IJ,J} \quad ,$$

the finite difference form of Eq. (22) yields:

$$z_{IJ+1,j}^{*(\ell)} - z_{IJ-1,j}^{*(r)} = z_{IJ+1,j} - z_{IJ-1,j} + \Delta s^2 [n_{xx}^{(r)} - n_{xx}^{(\ell)}]_{IJ,j} \ell_{IJ,j}^z \quad (23)$$

Then, solving Eqs. (21) and (23) for  $z_{IJ-1,j}^{*(r)}$ , we obtain

$$z_{IJ-1,j}^{*(r)} = z_{IJ-1,j} + \frac{\Delta s^2}{2} [n_{xx}^{(\ell)} - n_{xx}^{(r)}]_{IJ,j} \ell_{IJ,j}^z \quad (24)$$

where the square bracket is related to the jump in  $y_w''$  at IJ. Since  $\ell^z$  can be quite large, the last term on the right in Eq. (24) is not negligible. Hence, using  $z_{IJ-1,j}$  in place of  $z_{IJ-1,j}^{*(r)}$  could lead to a noticeable error.

### III. NUMERICAL RESULTS

#### Problem Geometry and Numerical Solution Procedure

The wall geometry of the diffuser or nozzle is defined by the same equation as in Reference 2, namely

$$y_w(x) = \left\{ \begin{array}{ll} 0 & , \quad x_0 \leq x \leq 0 \\ Ax^2(3-2x) & , \quad 0 \leq x \leq 1 \\ A & , \quad 1 \leq x \leq x_f \end{array} \right\} \quad (25)$$

where A is the change in height between the leading and trailing edges of the cubic transition section. For a diffuser, A is negative and for a nozzle it is positive. An additional geometric parameter is H, the throat half height. The geometry is shown in Figure 1.

The numerical solution procedure for the Navier-Stokes equations and parabolized vorticity approximation is identical, as described in Section II. The details of the Blasius starting solution, the initial guess and SLOR procedure are given in Reference 1.

In the present work a "consistent form" of the parabolized vorticity approximation is used by which is meant the following:

1. At map junctions the averaged form of the vorticity equation, given by Eq. (16), is used with  $\bar{\zeta}_{ss}$  omitted.
2. One step downstream of a map junction, second-order accuracy in the s-direction is maintained in the convective terms by use of Eq. (24).

In the "consistent form," as in Reference 1, one step downstream of the starting solution the convective derivatives are approximated by first-order accurate backward formulas to avoid the necessity of two starting profiles.

#### Comparison of Navier-Stokes and Parabolized Vorticity Approximation Solutions

Three cases were run to compare SFD results for the Navier-Stokes equations with the parabolized vorticity approximation. The problem parameters for these cases are given in Table 1 below:

Case No.	Re	A	H	$x_0$	$x_f$	$x_s$	$\Delta x$	RF1	RF2
1	1000	-0.15	1.0	-1.0	2.0	1.0	0.2	1.0	1.0
2	10,000	-0.075	0.25	-1.0	3.0	1.0	0.2	1.0	0.6
3	1000	0.10	1.0	-2.0	3.0	1.0	0.2	1.2	1.0

Table 1. Problem Parameters.

In Table 1,  $x_s$  denotes the distance from the initial line, at  $x_0$ , to the leading edge of the initial flat plate.

For all three cases, 20 nonuniformly spaced intervals were used in the  $n$ -direction with 11 points in the Blasius starting solution. The  $n$  nodal spacing was generated with the step size ratio  $\sigma = 1.1$  in the Blasius solution and with  $\sigma$  adjusted slightly in the outer uniform flow region to give 10 intervals. This same procedure was used in Reference 1. The convergence tolerance in the relaxation solution, as described in Reference 1, was taken to be unity in all three cases.

Detailed comparisons of numerical results between the parabolized vorticity and Navier-Stokes solutions for the three cases are presented in Tables 2-7. These tables show wall friction coefficient and wall pressure coefficient. In all cases, results for the consistent parabolized vorticity approximation are given. For Case 1 only, results for the original form of the parabolized vorticity approximation, as described in Reference 1, were also obtained. Tables 2-7 show that the difference between consistent parabolized vorticity approximation and Navier-Stokes results for  $c_f$  and  $c_p$  are negligible everywhere. For Case 1, Tables 2 and 3 show that the original parabolized vorticity approximation and Navier-Stokes solutions differ significantly at  $x = 0.2$ , one step downstream of the diffuser leading edge. This disagreement is most likely caused by the first-order accurate  $s$ -differencing used in the convective terms of the original parabolized vorticity approximation.

Plots of convergence history for the three cases are presented in Figures 2-4. In all cases the initial flow field guess and relaxation factors were the same for the parabolized vorticity approximation and Navier-Stokes solutions. These plots show that the extra terms in the equation between parabolized vorticity and Navier-Stokes make essentially no difference in the convergence.

Comparison with Results of Inoue

Inoue [2] has also solved numerically laminar flow in a two-dimensional diffuser, the same configuration treated here and in Reference 1. Although a nearly identical shearing transformation is used, the equations solved are somewhat different as are the numerics and method of solution.

Inoue uses a displacement body approach with parabolized viscous equations solved in place of the standard first-order boundary-layer equations. In the inviscid outer flow, the solution of Laplace's equation gives the velocity at the edge of the viscous layer. The viscous and inviscid problems are solved alternately until convergence is reached.

The parabolization is performed before the shearing transformation is applied which is opposite the present treatment. Thus, if

$$h(x) = y_w(x) - y_e \quad , \quad (26)$$

and

$$\eta = 1 - n \quad , \quad (27)$$

then working out the metric coefficients, the present parabolized vorticity equation is,

$$\frac{1}{h}(\psi_\eta \zeta_s - \zeta_\eta \psi_s) = \frac{1}{\text{Re}} \left[ \left( \frac{1 + h'^2 \eta}{h^2} \right) \zeta_{\eta\eta} + \left( \frac{2h' h'' - h'''}{h^2} \right) \eta \zeta_\eta \right] \quad , \quad (28)$$

whereas the equation used by Inoue is,

$$\frac{1}{h}(\psi_\eta \zeta_s - \zeta_\eta \psi_s) = \frac{1}{\text{Re} h^2} \zeta_{\eta\eta} \quad . \quad (29)$$

Inoue discretizes his governing equations using second-order accurate finite differences. The parabolized vorticity equation was differenced in such a way as to account for the direction of the x-component of velocity which was not found to be necessary here. For both the viscous and inviscid regions, he used a constant step size in both transformed directions with a grid of 141 (in s) by 41 (in n) nodes. His computational zone length was seven units which gave  $\Delta s = 0.05$ .

For comparison with results given in Inoue's Figure 12, two Reynolds numbers were chosen. The parameters describing the problem as given in Table 8 below.

A	H	$x_0$	$x_f$	$x_s$	$\Delta x$	RF1	RF2
-0.08	1.0	-1.0	3.0	2.0	0.10	1.0	1.0

Table 8. Diffuser Parameters for Comparison with Inoue

The Reynolds numbers were 6250 in Case 4 and 1000 in Case 5, which represent flows with and without a separation bubble. Only consistent PVA results were run for these cases. The convergence tolerance was tightened to 0.1 which required 107 and 62 iterations for convergence in Cases 4 and 5, respectively. After a tolerance of 1.0 is reached the convergence markedly slows down which is characteristic of the relaxation process.

Comparisons with Inoue's results are presented in Figures 5 and 6 or Cases 4 and 5, respectively. The agreement in both cases is quite good although some discrepancy does show up in the diffuser proper where the shearing transformation takes effect. The slight disagreement here is most likely caused by the different parabolizations used rather than by a step size effect. By examining the present numerical results closely, the second term on the right side of Eq. (28), proportional to  $\zeta_{\eta}$ , has been found not to be negligible compared to the first term, proportional to  $\zeta_{\eta\eta}$ , and results from Cases 1-3 bear this out.

No comparisons can be given on the efficiency of Inoue's approach in contrast to the present one because no convergence information is given in Reference 2 for the diffuser solutions.

#### IV. CONCLUSIONS

The following conclusions can be drawn from this study for the particular problem considered:

1. All parameters being the same, the consistent parabolized vorticity approximation described in Section II, gives nearly identical numerical results to the Navier-Stokes equations. Thus, mild non-orthogonality of the coordinate system, introduced by a shearing transformation, has negligible effect on the parabolized solution.
2. For line relaxation there is practically no difference in convergence properties of the Navier-Stokes equations and parabolized vorticity approximation.
3. The consistent parabolized vorticity approximation gives results in much closer agreement with the Navier-Stokes equations than does the original form used in Reference 1. The reason appears to be the increased accuracy of the former one step downstream of map junctions.
4. Comparison of consistent parabolized vorticity approximation results for wall friction coefficient with those of Inoue [2] show good agreement with detectable differences occurring in the diffuser section. The reason for these differences is most likely due to the different parabolizations used. In light of conclusion 1, the present procedure, in which the vorticity equation is parabolized after transformation, is the better approximation.

REFERENCES

1. Hoffman, G. H., "A Spline Solution of the Incompressible Parabolized Navier-Stokes Equations in a Sheared Coordinate System," TM 82-51, Applied Research Laboratory, The Pennsylvania State University, 25 January 1982.
2. Inoue, Osamu, "Numerical Investigation of Two-Dimensional, Incompressible Boundary Layer Flows with Separation and Reattachment," ISAS Rept. No. 582 (Vol. 45, No. 7), Inst. of Space and Aeron. Sci., University of Tokyo, Japan (1980).

Sta.	x	WALL FRICTION COEFFICIENT		
		Original PVA	Consistent PVA	Navier-Stokes
1	-1.0	.021002	.021002	.021002
2	-0.8	.021174	.021156	.021077
3	-0.6	.020821	.020786	.020701
4	-0.4	.020545	.020482	.020387
5	-0.2	.020842	.020727	.020602
6	0.0	.023059	.022841	.022717
7	0.2	.014322	.013027	.012764
8	0.4	.003817	.003324	.003081
9	0.6	-.000331	-.000540	-.000689
10	0.8	-.001570	-.001699	-.001843
11	1.0	-.001517	-.001725	-.001907
12	1.2	-.000222	-.000542	-.000741
13	1.4	.001290	.000939	.000750
14	1.6	.002787	.002436	.002260
15	1.8	.004161	.003835	.003675
16	2.0	.005414	.005125	.005012

Table 2. Wall Friction Coefficient, Case 1.



Sta.	x	WALL PRESSURE COEFFICIENT		
		Original PVA	Consistent PVA	Navier-Stokes
1	-1.0	0	0	0
2	-0.8	-.005094	-.005068	-.005147
3	-0.6	-.016517	-.016407	-.016563
4	-0.4	-.030148	-.029870	-.029984
5	-0.2	-.047103	-.046395	-.046318
6	0.0	-.073750	-.072556	-.072530
7	0.2	-.084109	-.075889	-.075375
8	0.4	-.059274	-.044703	-.042874
9	0.6	-.027230	-.12197	-.009627
10	0.8	-.003817	.011095	.013962
11	1.0	.014969	.030059	.033431
12	1.2	.031811	.047487	.051499
13	1.4	.046000	.062511	.067099
14	1.6	.056420	.073774	.078830
15	1.8	.063076	.081232	.086662
16	2.0	.066304	.085177	.090908

Table 3. Wall Pressure Coefficient, Case 1

Sta.	x	WALL FRICTION COEFFICIENT	
		Consistent PVA	Navier-Stokes
1	-1.0	.0066413	.0066413
2	-0.8	.0066338	.0066320
3	-0.6	.0064226	.0064210
4	-0.4	.0061799	.0061784
5	-0.2	.0060107	.0060090
6	0.0	.0062597	.0062582
7	0.2	.0029994	.0029893
8	0.4	.0002452	.0002380
9	0.6	-.0005525	-.0005538
10	0.8	-.0007590	-.0007613
11	1.0	-.0009366	-.0009408
12	1.2	-.0011086	-.0011139
13	1.4	-.0010899	-.0010960
14	1.6	-.0009775	-.0009843
15	1.8	-.0008091	-.0008163
16	2.0	-.0006033	-.0006108
17	2.2	-.0003785	-.0003861
18	2.4	-.0001506	-.0001581
19	2.6	.0000689	.0000617
20	2.8	.0002732	.0002662
21	3.0	.0004609	.0004545

Table 4. Wall Friction Coefficient, Case 2.

Sta.	x	WALL PRESSURE COEFFICIENT	
		Consistent PVA	Navier-Stokes
1	-1.0	0	0
2	-0.8	-.004503	-.004517
3	-0.6	-.013959	-.013996
4	-0.4	-.023760	-.023811
5	-0.2	-.033833	-.033890
6	0.0	-.048304	-.048393
7	0.2	-.040744	-.040768
8	0.4	-.008176	-.008079
9	0.6	.016028	.016110
10	0.8	.029595	.029633
11	1.0	.040106	.040146
12	1.2	.051999	.052060
13	1.4	.066015	.066108
14	1.6	.080605	.080736
15	1.8	.094879	.095053
16	2.0	.10831	.10853
17	2.2	.12050	.12077
18	2.4	.13126	.13157
19	2.6	.14051	.14088
20	2.8	.14834	.14875
21	3.0	.15485	.15529

Table 5. Wall Pressure Coefficient, Case 2

Sta.	x	WALL FRICTION COEFFICIENT	
		Consistent PVA	Navier-Stokes
1	-2.0	.021002	.021002
2	-1.8	.020719	.020650
3	-1.6	.019930	.019867
4	-1.4	.019012	.018954
5	-1.2	.018116	.018062
6	-1.0	.017269	.017219
7	-0.8	.016446	.016399
8	-0.6	.015587	.015542
9	-0.4	.014597	.014556
10	-0.2	.013317	.013285
11	0.0	.011326	.011262
12	0.2	.014672	.014507
13	0.4	.023851	.023556
14	0.6	.033256	.032949
15	0.8	.037465	.037297
16	1.0	.029313	.029191
17	1.2	.020060	.019966
18	1.4	.018175	.018120
19	1.6	.017424	.017375
20	1.8	.017015	.016969
21	2.0	.016707	.016660
22	2.2	.016426	.016381
23	2.4	.016159	.016112
24	2.6	.015895	.015849
25	2.8	.015636	.015587
26	3.0	.015369	.015366

Table 6. Wall Friction Coefficient, Case 3.

Sta.	x	WALL PRESSURE COEFFICIENT	
		Consistent PVA	Navier-Stokes
1	-2.0	0	0
2	-1.8	-.00380	-.00391
3	-1.6	-.01178	-.01205
4	-1.4	-.01979	-.02015
5	-1.2	-.02700	-.02745
6	-1.0	-.03326	-.03378
7	-0.8	-.03845	-.03904
8	-0.6	-.04234	-.04299
9	-0.4	-.04440	-.04513
10	-0.2	-.04374	-.04456
11	0.0	-.03847	-.03913
12	0.2	-.04303	-.04271
13	0.4	-.08784	-.08551
14	0.6	-.18239	-.17801
15	0.8	-.29729	-.29251
16	1.0	-.36802	-.36381
17	1.2	-.37540	-.37113
18	1.4	-.36578	-.36125
19	1.6	-.36480	-.36023
20	1.8	-.36728	-.36271
21	2.0	-.37158	-.36703
22	2.2	-.37686	-.37233
23	2.4	-.38263	-.37810
24	2.6	-.38859	-.38408
25	2.8	-.39456	-.39006
26	3.0	-.40043	-.39587

Table 7. Wall Pressure Coefficient, Case 3.

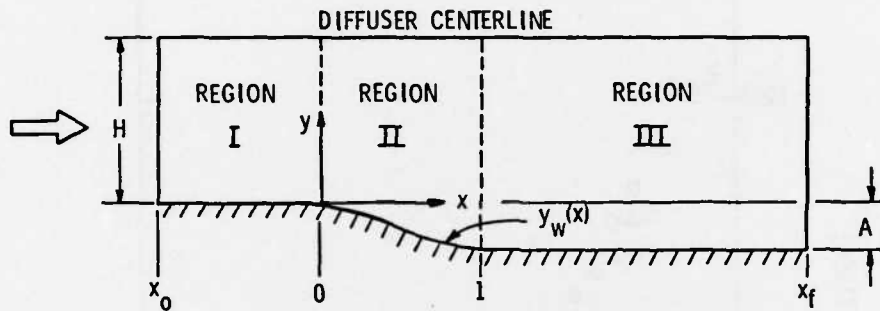


Figure 1. Problem Geometry

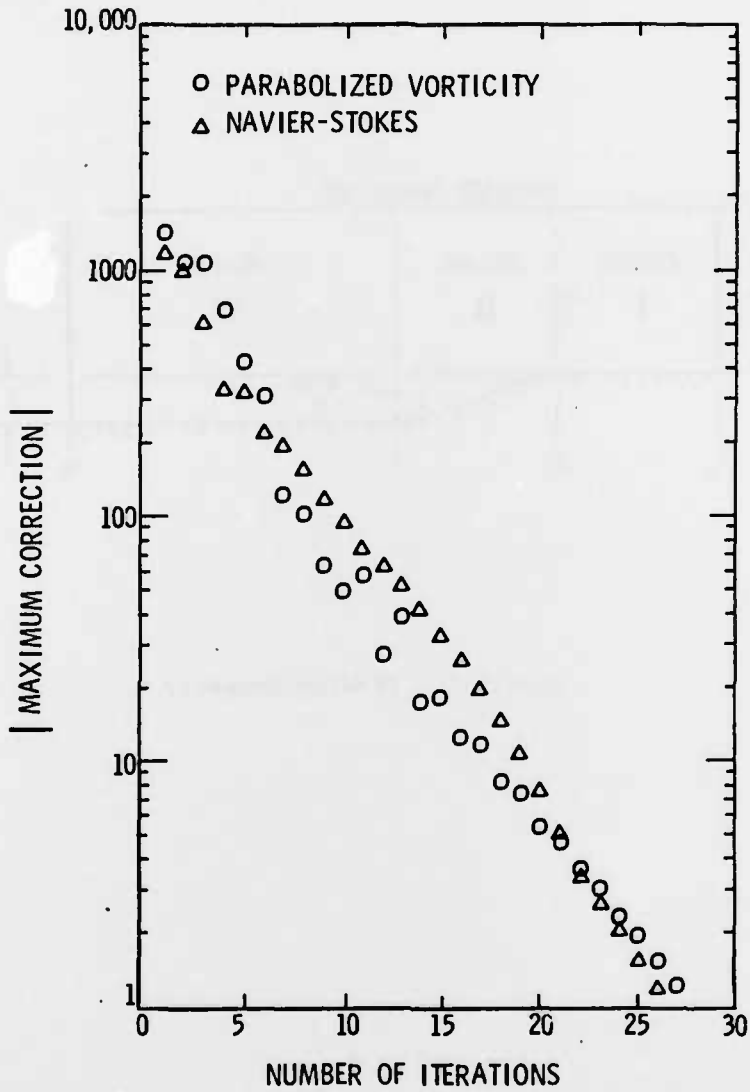


Figure 2. Convergence History, Case 1.

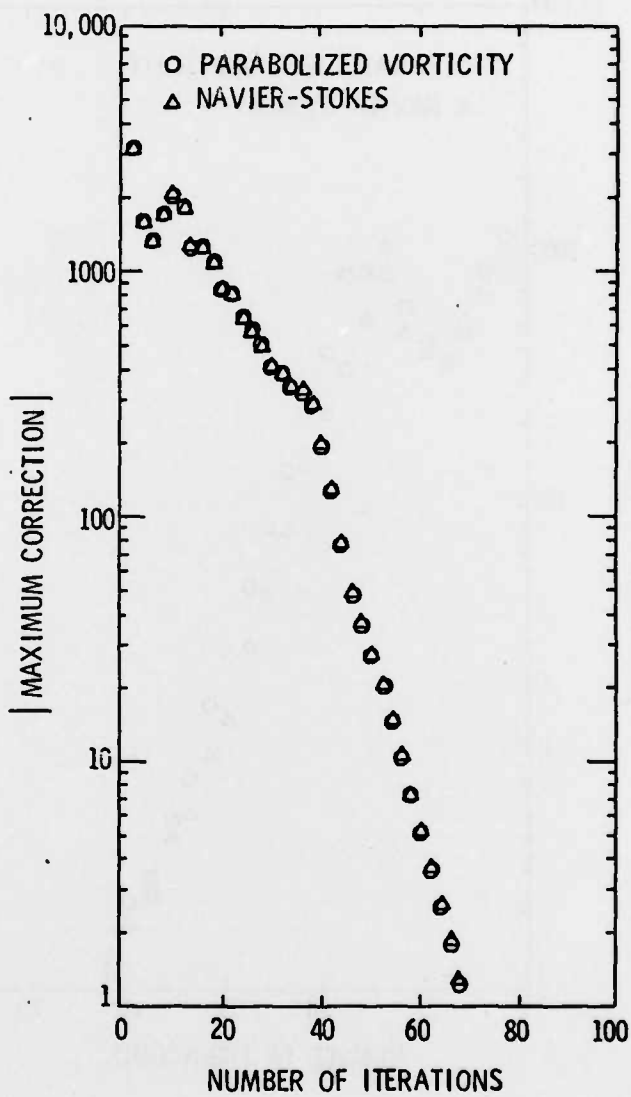


Figure 3. Convergence History, Case 2.



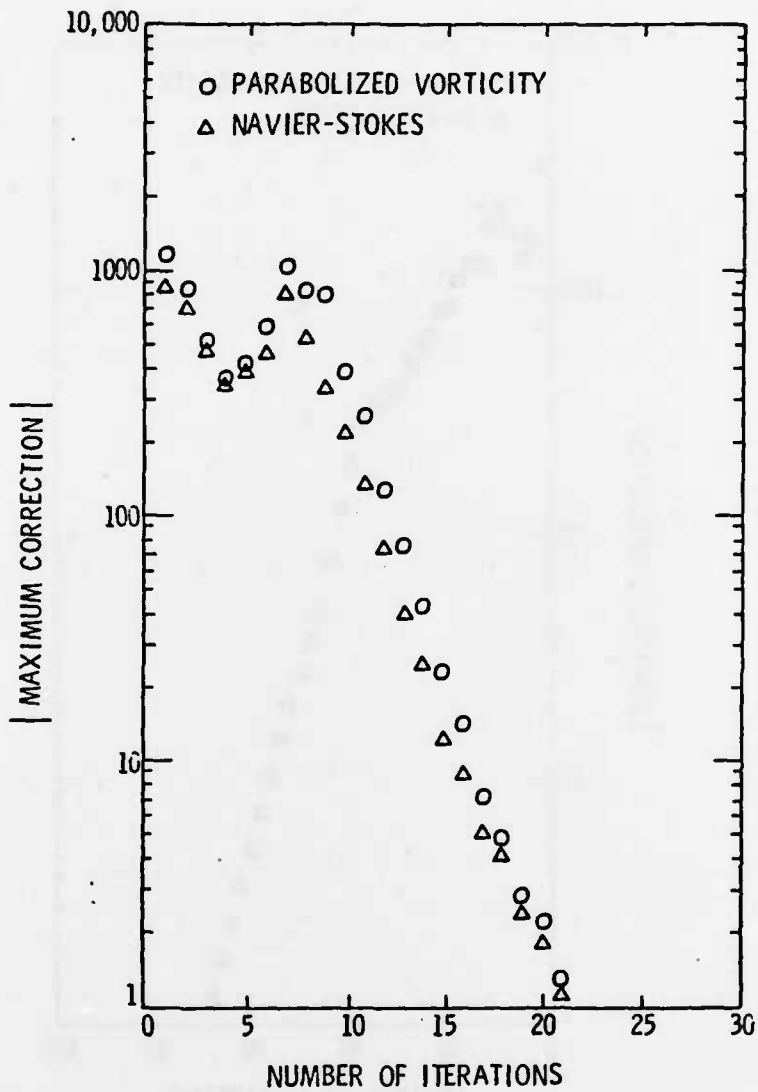


Figure 4. Convergence History, Case 3.

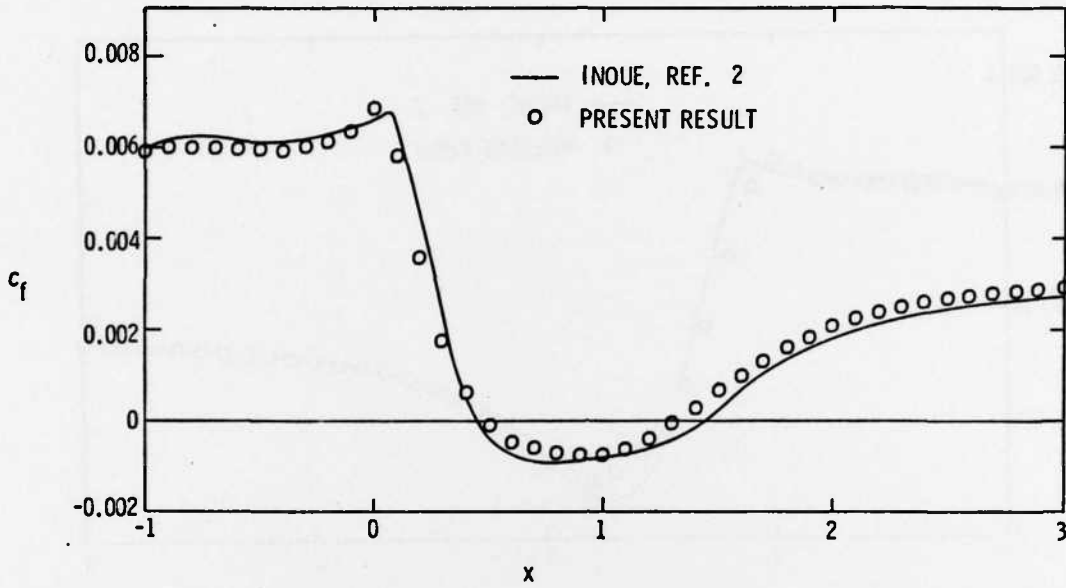


Figure 5. Wall Friction Coefficient Comparison, Case 4.

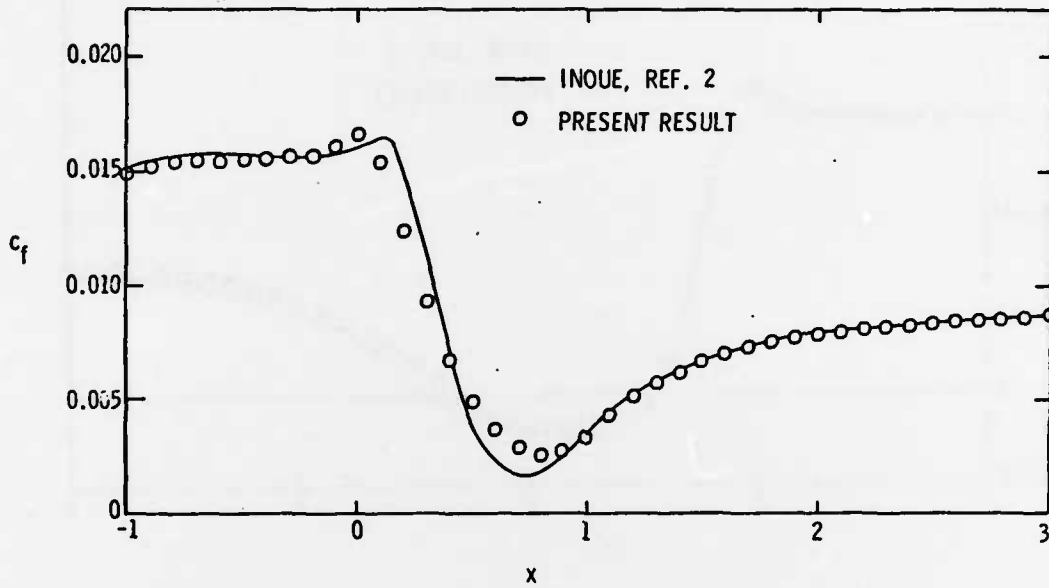


Figure 6. Wall Friction Coefficient Comparison, Case 5.

DISTRIBUTION LIST FOR UNCLASSIFIED TM 82-72 by G. H. Hoffman, dated  
17 February 1982

Commander  
Naval Sea Systems Command  
Department of the Navy  
Washington, DC 20362  
Attn: T. E. Pearce  
Code NSEA-63R31  
(Copy No. 1)

Commander  
Naval Underwater Systems Center  
Newport, RI 02840  
Attn: D. Goodrich  
Code 2634  
(Copy No. 2)

Commander  
David W. Taylor Naval Ship R&D Center  
Department of the Navy  
Bethesda, MD 20084  
Attn: T. T. Huang  
Code 1552  
(Copy No. 3)

Commander  
Naval Surface Weapons Center  
Silver Spring, MD 20910  
Attn: W. J. Glowacki  
Code R-44  
(Copy No. 4)

Office of Naval Research  
Department of the Navy  
Arlington, VA 22217  
Attn: H. Fitzpatrick  
Code 438  
(Copy No. 5)

Office of Naval Research  
Attn: A. H. Gilmore  
(Copy No. 6)

Defense Technical Information Center  
5010 Duke Street  
Cameron Station  
Alexandria, VA 22314  
(Copy Nos. 7 through 12)

Naval Research Laboratory  
Washington, DC 20390  
Attn: Library  
(Copy No. 13)

Superintendent (Code 1424)  
Naval Post Graduate School  
Monterey, CA 93949  
(Copy No. 14)

NASA Lewis Research Center  
21000 Brookpark Road  
Cleveland, OH 44135  
Attn: W. N. McNally  
MS 5-9  
(Copy No. 15)

Professor P. K. Khosla  
Department of Aerospace Engineering and  
Applied Mechanics  
University of Cincinnati  
Cincinnati, OH 45221  
(Copy No. 16)

Professor C. L. Merkle  
The Pennsylvania State University  
Department of Mechanical Engineering  
University Park, PA 16802  
(Copy No. 17)

The Pennsylvania State University  
APPLIED RESEARCH LABORATORY  
P. O. Box 30  
State College, PA 16801  
Attn: R. E. Henderson  
(Copy No. 18)

Applied Research Laboratory  
Attn: S. A. Abdullah  
(Copy No. 19)

Applied Research Laboratory  
Attn: D. W. Prather  
(Copy No. 20)

Applied Research Laboratory  
Attn: G. C. Lauchle  
(Copy No. 21)

Applied Research Laboratory  
Attn: W. S. Gearhart  
(Copy No. 22)

Applied Research Laboratory  
Attn: M. R. Sheller  
(Copy No. 23)

Applied Research Laboratory  
Attn: G. H. Hoffman  
(Copy No. 24)

Applied Research Laboratory  
Attn: Garfield Thomas Water Tunnel Files  
(Copy No. 25)

**DATE**  
**FILME**